High-pressure Raman scattering study of ferroelectric $K_3Nb_3O_6(BO_3)_2$

M. Maczka,[1] W. Paraguassu,[2] P. T. C. Freire,[3] A. G. Souza Filho,[3] J. Mendes Filho,[3] and J. Hanuza[4]
[1]*Institute of Low Temperature and Structure Research, Polish Academy of Sciences, P.O. Box 1410, 50-950 Wroclaw 2, Poland*
[2]*Departamento de Fisica, Universidade Federal do Maranhão, São Luis 65085-580, MA, Brazil*
[3]*Departamento de Fisica, Universidade Federal do Ceara, P.O. Box 6030, Fortaleza 60455-900, CE, Brazil*
[4]*Department of Bioorganic Chemistry, University of Economics, 53-345 Wroclaw, Poland*
(Received 9 April 2010; revised manuscript received 17 June 2010; published 9 July 2010)

Polarized Raman scattering studies and lattice-dynamics calculations were performed at ambient pressure and temperature. These results allowed us to propose the normal-mode symmetries and assignments. High-pressure Raman scattering studies were further performed revealing the onset of two reversible phase transformations near 1.2 and 4.5 GPa with different structural characteristics. The pressure dependence of Raman bands provides strong evidence that the first phase transition involves significant shifts of the potassium atoms associated with small shifts of the niobium atoms whereas the second phase transition is associated mainly with significant shifts of the Nb atoms toward the center of the NbO_6 octahedra. In the structure stable above 4.5 GPa the Nb atoms are dynamically disordered among symmetry equivalent positions.

DOI: 10.1103/PhysRevB.82.014106 PACS number(s): 78.30.Hv, 77.84.Ek, 77.80.B−

I. INTRODUCTION

Boron containing compounds play an important role in modern nonlinear optics since these materials usually have high $\chi^{(2)}$ and $\chi^{(3)}$ nonlinear susceptibilities, outstanding resistance to laser damage, and a cutoff wavelength in the near-ultraviolet region.[1–4] $K_3Nb_3O_6(BO_3)_2$ (KNBO) has been found to be a $\chi^{(3)}$-active crystal for picosecond stimulated Raman scattering generation in the visible and near-infrared (IR) region.[5]

KNBO crystallizes above 783 K in $P\bar{6}2m$ structure, consisting of triple groups of NbO_6 octahedra linked by planar BO_3 triangles.[6,7] The main feature of this structure is the presence of large pentagonal cavities occupied by the K atoms. The ionic conductivity and dielectric studies showed that this borate exhibits superionic properties at elevated temperatures.[8,9] It was also shown that KNBO exhibits successive ferroelastic and ferroelectric phase transitions below 783 K, and its structure at room temperature was suggested to be $P2_1ma$.[7–9] However, it was emphasized by other authors that the direction of the spontaneous polarization does not agree with the $P2_1ma$ symmetry and therefore this symmetry is not completely determined.[8,9] Symmetries of the remaining phases are also not yet resolved. Our recent temperature-dependent Brillouin scattering studies revealed the presence of very intense quasielastic light scattering, i.e., the so-called central peaks and unusually strong damping of acoustic modes at high temperatures.[10] The observed behavior was attributed to melting of the potassium sublattice as a result of the order-disorder phenomenon driven phase transitions. It was also shown that the temperature-induced phase transitions at 750, 690, and 388 K are mainly of order-disorder type.[10] We have also reported temperature-dependent Raman scattering and IR studies, which revealed changes in the distortion of the NbO_6 octahedra at the 185 and 385 K phase transitions.[11]

In situ temperature studies show that this ferroelectric and superionic material has very complex polymorphism, which is still not well understood. Pressure is another useful thermodynamic variable that can provide information on mechanism of the phase transitions and origin of lattice instabilities because this parameter drastically affects both bond lengths and bond angles. Therefore, to better understand the nature of lattice instabilities in this crystal, it is necessary to access its properties also as a function of pressure using Raman spectroscopy. This paper reports lattice-dynamics (LD) calculations and high-pressure Raman spectroscopy studies of KNBO single crystal indicating that KNBO exhibits two structural phase transitions near 1.2 and 4.5 GPa. The first phase transition is accompanied by significant changes in the potassium sublattice whereas the second one involves mainly the NbO_6 octahedral framework.

II. EXPERIMENTAL AND MODELING

The KNBO crystals were grown from a flux. The mixture of K_2CO_3, Nb_2O_5, and B_2O_3, corresponding to the composition KNBO and $K_2B_4O_7$ in a ratio 1:1, was heated to 1000 °C, kept at this temperature for 40 h, cooled at a rate 2 °C/h to 840 °C, and then cooled at a rate 10 °C to room temperature. Details can be found elsewhere.[10]

The high-pressure Raman spectra were measured with a triple-grating spectrometer Jobin Yvon T64000, equipped with a N_2-cooled charge-coupled-device detection system. The line 514.5 nm of an argon laser was used as excitation. An Olympus microscope lens with a focal distance $f=20.5$ mm and a numeric aperture of NA=0.35 was used to focus the laser beam on the sample surface. High-pressure experiments were performed using a diamond-anvil cell with a 4:1 methanol-ethanol mixture as a pressure-transmitting medium. Pressures were measured using shifts of the ruby R1 and R2 fluorescence lines.[12] The spectrometer slits were set for a resolution of 2 cm^{-1}.

LD calculations were performed using GULP code developed by Gale.[13] We have chosen a set of classical ionic pair potential that better optimize the KNBO structure ($P\bar{6}2m$ space group). Potential parameters were used to derive the initial force constants used in the phonon calculations. The

TABLE I. Potential parameters (see equations in the text) and ionic charges used in the lattice-dynamics calculation. Charges (e), $Z_K=1$; $Z_B=3$; $Z_{Nb}=5$; $Z_O=-2.0$.

	b (eV)	ρ (Å)	c (eV Å^6)
K-O	958.21	0.3606	0
B-O	40765.1	0.138	1.34
O-Nb	3823.184	0.3	0
O-O	25.41	0.6937	32.32

ionic shell model used in the GULP code treats the material as a collection of core-shell systems (accounting for nuclei and electron shell) interacting through electrostatic and short-range classic potentials. This model was successfully used for a number of molybdate- and tungstate-based systems.[14–16] The following interatomic potential is taken into account:

$$U_{ij}(r_{ij}) = \frac{z_i z_j e^2}{r_{ij}} + b_{ij} \exp\left[\frac{-r_{ij}}{\rho_{ij}}\right] - \frac{c_{ij}}{r_{ij}^6}. \quad (1)$$

The first term describes the Coulomb forces for modeling the long-range interactions where z_i and z_j are the effective charges of the i and j ions, respectively, separated by the distance r_{ij}. The second term is related to the Born-Mayer-type repulsive interaction for the short-range forces using parameters ρ_{ij} and b_{ij}, which correspond to the ionic radii and ionic stiffness, respectively. A van der Waals attractive interaction (third term) is related to the dipole-dipole interaction. The initial lattice parameters and atomic positions for the KNBO structure were taken from the experimental data.[6] The potential parameters and ionic charges used in our calculation, listed in Table I, show good agreement between the calculated and experimental lattice parameters, obtaining volumetric error within 1%.

The phonon calculations were performed using Wilson's **GF** matrix method, sometimes referred to as FG method and the software package VIBRATZ developed by Dowty.[17] The matrix $\mathbf{G^{-1}}$ gives the kinetic energy in terms of arbitrary linear internal coordinates while **F** represents the potential energy in terms of these coordinates. The initial force constants were obtained using the relation

$$f_{ij} = -\frac{1}{r}\frac{\partial U_{ij}(r)}{\partial r}, \quad (2)$$

where the indices i and j refer to interacting ions separated by a distance r. The force constant values for Nb-O1 and O3-O3 bonds were refined to fit the experimental data (the final values: 0.79 mdyn/Å and 1.27 mdyn/Å, respectively), a necessity in order to correct for the lack of covalence in the ionic model. Additionally, we have introduced an out-of-plane bonding force, 0.35 mdyn/Å, for the borate molecular group (BO_3), which is called "psi bond-plane angle" in the VIBRATZ code. Force-constant values used in LD calculations for KNBO crystal are presented in Table II and the calculated and experimental Raman and IR wave numbers are listed in Table III.

TABLE II. Force-constant values for KNBO crystal used in LD calculations.

Bonds	Bond length (Å)/force constant (mdyn/Å)
B-O	1.36/3.80
	3.7–3.8/0.24
O-O	2.36/1.27
	2.75–2.92/0.47
K-O	2.78–2.95/0.14
Nb-O	1.94–2.0/1.53
	3.75–3.84/0.43–0.24

III. RESULTS AND DISCUSSION

A. Crystal structure and lattice dynamics of $K_3Nb_3O_6(BO_3)_2$

The crystal structure of KNBO is built up of chains of NbO_6 octahedra running along the c axis and linked by O1 oxygen atoms (see Fig. 1). These chains are linked in the ab plane by shared O2 atoms, spaces between the NbO_6 octahedra are empty. These triple chains are then connected by BO_3 triangles forming a three-dimensional structure. A peculiar characteristic of this structure is the presence of large pentagonal prismatic cavities occupied by the K atoms. The room-temperature structure was suggested to be orthorhombic, $P2_1ma$. Since this symmetry is not certain, it is convenient to start the analysis from the parent hexagonal phase, space group $P\bar{6}2m$. This approximation is reasonable since the ambient pressure and room-temperature structure is only a slight modification of its parent hexagonal phase, i.e., the x-ray analysis showed that the hexagonal-orthorhombic distortion of the lattice constants is only 0.01%.[7]

A standard group theoretical analysis for the $P\bar{6}2m$ phase of KNBO containing 20 atoms in the unit cell leads to 60 degrees of freedom at the Brillouin-zone center (Γ point). The optical modes are distributed among the irreducible representations of the factor group D_{3h} as $6A_1'+6A_2'+2A_1''+6A_2''+14E'+6E''$. Selection rules state that A_1' and E'' modes are Raman active, A_2'' modes are IR active, E' modes are both Raman and IR active whereas the A_2' and A_1'' modes are not active.

The polarized Raman spectra at room temperature and ambient pressure are shown in Fig. 2. This figure shows that the bands are observed in a few well-separated regions. The highest wave number Raman (IR) modes in the range 1201–1240 cm^{-1} (1208–1313 cm^{-1}) and near 1067 cm^{-1} can be unambiguously assigned to the antisymmetric (ν_3) and symmetric (ν_1) stretching modes of the BO_3 units. According to literature data the out-of-plane bending (ν_2) and in-plane bending (ν_4) modes of the BO_3 group were observed around 670–800 cm^{-1} and 590–660 cm^{-1}, respectively.[18–20] These modes were usually very weak or weak in Raman spectra and much more intense in IR spectra.[18–20] Our LD calculations indicate that the weak and narrow Raman (IR) band at 698 (695) cm^{-1} can be assigned to the ν_2 mode. The ν_4 mode is not observed in the Raman spectra but it gives rise to strong IR band at 631 cm^{-1}. The Raman spectra show also presence of the band at 645 cm^{-1},

TABLE III. Experimental and calculated wave numbers for hexagonal phase of KNBO together with the proposed assignment.

Calculated						Experimental		
A_1'	A_2'	A_1''	A_2''	E'	E''	Raman	IR (Ref. 11)	Assignment
				1244		1240	1313	$\nu_3(BO_3)$
				1231		1201	1208	$\nu_3(BO_3)$
1068	1029					1067		$\nu_1(BO_3)$
						856	826	?
				754		776	786	NbO_6 stretching (mainly O2)
	717							NbO_6 stretching (mainly O2)
		668	693		688	698	695	$\nu_2(BO_3)$
			663		652	646		NbO_6 stretching (mainly O1)
				622			631	$\nu_4(BO_3)$
				582				$\nu_4(BO_3)$
556								NbO_6 stretching (mainly O2)
						474		
				455			424	
					418	433		
		398				410		$T'(BO_3)$
				414		388		
			348				368	
	365			367	344		337	
				324		328		
367						317		
312						297		
				309		289	286	NbO_6 bending and $L(BO_3)$
						272		
						257		
						250	240	
			230			245		
	215					220	215	$T'(Nb)$ and $L(BO_3)$
227						214	171	
				190		179		
	176					166		
				142		150	147	
						146	144	
						143		
			129			138		
131						127		
						117		$T'(K^+)$
					123	114	108	
						110		
					119	90		
						85		
				73		79		
	56					44		

which is very intense in the $y(zz)y$ polarization. LD calculations indicate that this mode can be assigned to stretching mode of the NbO_6 octahedra, which involves mainly large motions of the O1 oxygen atoms in the direction parallel to the z axis. It is worth to note that similar strong Raman band was observed also for many other niobates in the range

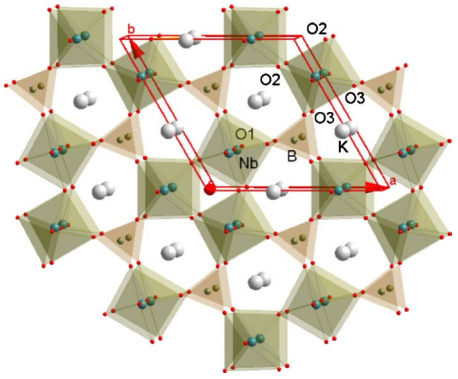

FIG. 1. (Color online) View of the KNBO crystal structure ($P\bar{6}2m$) along the c axis.

600–650 cm^{-1}.[21–24] Stretching modes of the NbO_6 octahedra, which involve mainly large motions of the O2 oxygen atoms in the direction perpendicular to the z axis, are observed at 776 (Raman) and 786 cm^{-1} (IR). The Raman spectra show also weak band at 856 cm^{-1}, which is observed only in the $y(xx)y$ polarization. A similar band was also observed for $KNbO_3$ and $NaNbO_3$ at 836 cm^{-1} and 868 cm^{-1}, respectively.[21,23] The origin of this band is not clear since it was assigned either as the LO component of the strongest Raman band or as a combination mode.[20,22]

In the low wave-number region, weak bands are observed below 180 cm^{-1} and in the 388–474 cm^{-1} range, whereas many bands in the 214–328 cm^{-1} range are of medium intensity. LD calculations indicate that the weak Raman bands in the 388–474 cm^{-1} range and below 170 cm^{-1} correspond to translational motions of the BO_3 groups and K^+ ions, respectively. It is worth noting however that the number of observed bands below 170 cm^{-1} is much larger than the calculated for the hexagonal symmetry. Some of these additional bands can be attributed to splitting of doubly degenerated modes of the hexagonal phase due to orthorhombic distortion. However, since the primitive cell of the room-temperature phase contains four times more KNBO units than the hexagonal phase, some of these low wave-number modes can also be attributed to folding of the Brillouin-zone boundary modes of the hexagonal phase into Brillouin-zone center of the orthorhombic phase. The remaining bands in the 179–337 cm^{-1} range correspond to bending modes of the NbO_6 octahedra or translations of Nb atoms coupled with librational modes of the BO_3 groups (see Table III).

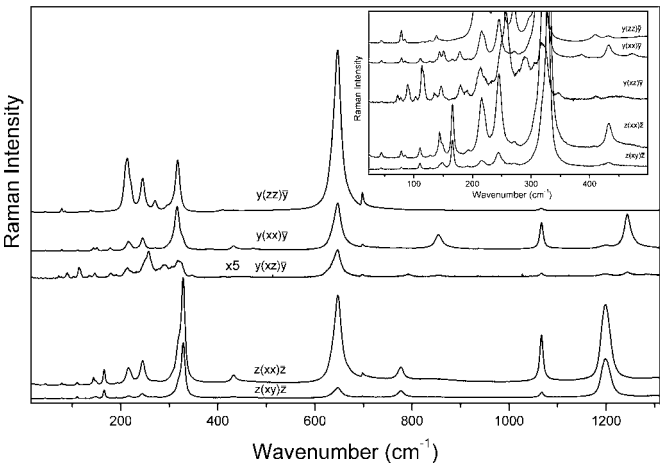

FIG. 2. Polarized Raman spectra of KNBO. The notation refers to hexagonal symmetry, i.e., the $y(zz)y$, $y(xx)y$, $y(xz)y$, $z(xx)z$, and $z(xy)z$ spectra correspond to A_1', $A_1'+E'$, E'', $A_1'+E'$, and E' modes of the high-temperature hexagonal phase, respectively. Differences between $y(xx)y$ and $z(xx)z$ are due to the fact that the actual structure deviates from hexagonal symmetry and is most probably orthorhombic. Inset shows details for weak bands in the 15–500 cm^{-1} range.

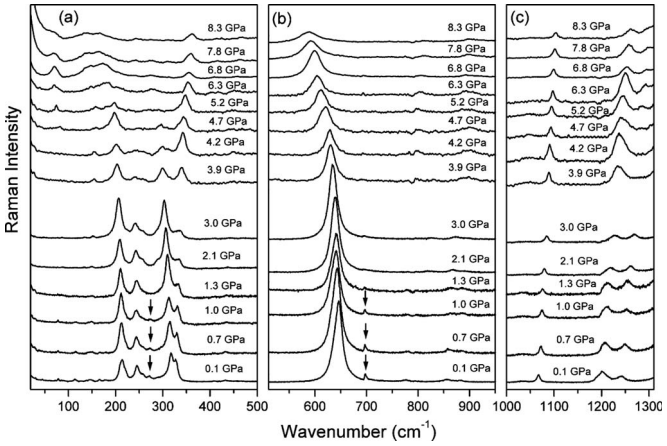

FIG. 3. Raman spectra of KNBO recorded at different pressures during compression experiments in the (a) low, (b) medium, and (c) high wave-number region. Arrows indicate the 271.6 (697.7) cm^{-1} band, which disappears (becomes very weak) near 1.2 GPa. Uncertainties in pressures are 0.1 GPa.

B. High-pressure Raman scattering studies

The Raman spectra recorded during compression experiments are presented in Fig. 3. However, the overall changes in the Raman spectra can be better followed by analyzing the wave number (ω) vs pressure (P) plot shown in Fig. 4. Figure 5 presents also pressure dependence of full width at half maximum (FWHM) of two bands. The mode wave numbers and FWHMs were evaluated by fitting the experimental spectra to Lorentzians (see Ref. 33). Figure 4 shows that the pressure dependence of all vibrational modes can be described by using a linear function $\omega(P)=\omega_0+\alpha P$. The values of ω_0 and α are summarized in Table IV. In general, with increasing pressure, the mode wave numbers increase (see Figs. 3 and 4). However, seven modes exhibit negative pressure dependence. The most significant softening in the first phase is observed for the 645.6, 317.2, and 245.4 cm^{-1} modes.

At 1.2 GPa the weak bands at 113.6, 165.6, 179.2, and 271.6 cm^{-1} disappear. The bands at 138.5 and 78.6 cm^{-1} shift to 133 and 88 cm^{-1} and become weak above 1.2 GPa. The intensity of the 697.7 cm^{-1} band significantly decreases. Furthermore, weak discontinuities in the pressure dependence of wave numbers are observed near 1.2 GPa for nearly all modes. These discontinuities are accompanied by a strong change in the slope of wave number vs pressure (Fig. 4).

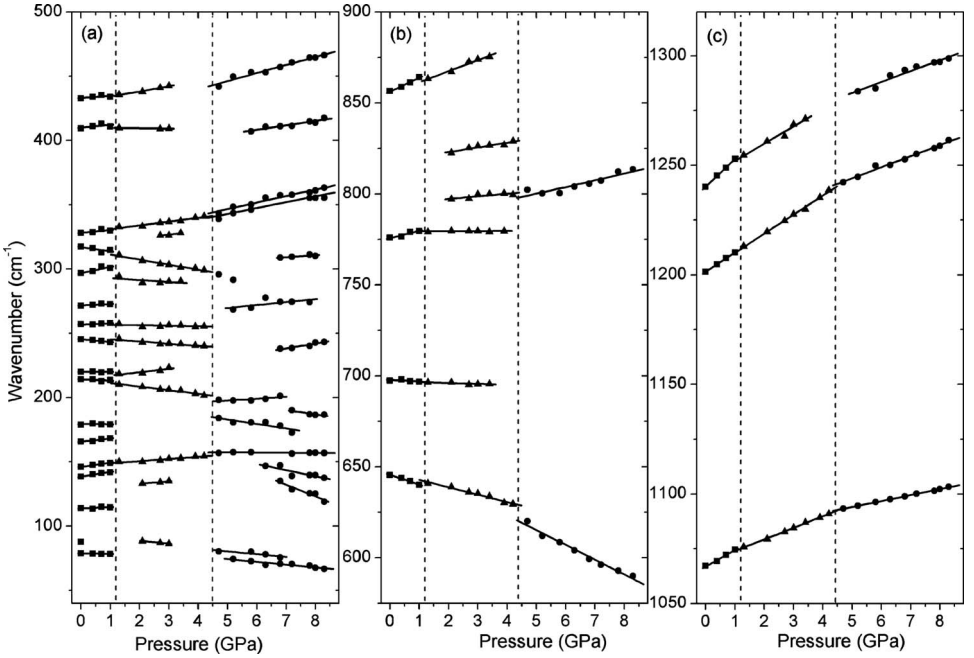

FIG. 4. Wave number vs pressure plots of the Raman modes observed in KNBO crystal for compression experiment. Uncertainties in mode wave numbers are smaller than size of the symbols, i.e., approximately 1.0 cm^{-1}. The vertical lines indicate the pressures at which KNBO undergoes phase transitions. The solid lines are linear fits on the data to $\omega(P)=\omega_0+\alpha P$.

Nearly all modes below 320 cm^{-1} exhibit negative pressure dependence above 1.2 GPa. These modifications of the Raman spectra indicate that a phase transformation takes place in KNBO near 1.2 GPa. Significant discontinuities in the pressure dependence of mode wave numbers are also observed near 4.5 GPa (Fig. 4). Furthermore, a number of bands disappear but also some bands appear. The most pronounced changes occur in the low wave-number region, below 300 cm^{-1}. The weak band near 88 cm^{-1} changes to a relatively intense band near 74 cm^{-1}, which exhibits significant softening upon application of pressure. Another much weaker band appears near 80 cm^{-1} and this shows weak softening. Intensity of the band near 300 cm^{-1} strongly decreases shifting toward lower wave numbers by about 23 cm^{-1}. The width of many Raman bands increases with increasing pressure. This broadening is especially well visible for the bands below 200 cm^{-1} and the most intense Raman band at 645.6 cm^{-1} (see Figs. 3 and 5). A wing appears below 80 cm^{-1} from scattering at zero frequency. The discussed modifications indicate that KNBO exhibits another structural transition at about 4.5 GPa.

Raman studies of KNBO crystal during decompression were also performed to access the reversibility of the phase transformations. Upon releasing pressure the spectrum of the starting phase was recovered (Fig. 6), thus indicating the reversibility of the process. However, intensities of some bands of the starting phase are different before increasing the pressure and after releasing the pressure. This difference is due to some slight reorientation of the sample during the pressure release and creation of defects in the compressed sample.[25,26]

C. Pressure-induced phase transitions

In order to understand the general behavior of KNBO crystal under pressure, it is important to provide a brief discussion of the structural changes induced by temperature (at ambient pressure). The structure at room temperature (assumed to have $P2_1ma$ symmetry) considerably differs from that at 823 K ($P\bar{6}2m$ symmetry) by the positions of the K atoms, i.e., at room temperature the K atoms are significantly shifted from the center of the potassium-oxygen polyhedra within the *ab* plane.[6,7] The NbO_6 octahedra are also affected, i.e., they are significantly more distorted at room tempera-

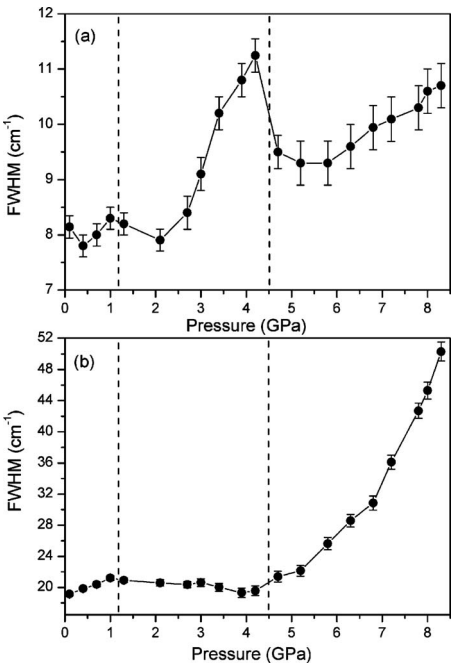

FIG. 5. Pressure dependence of FWHM for two representative modes at 1066.9 [panel (a)] and 645.6 cm^{-1} [panel (b)].

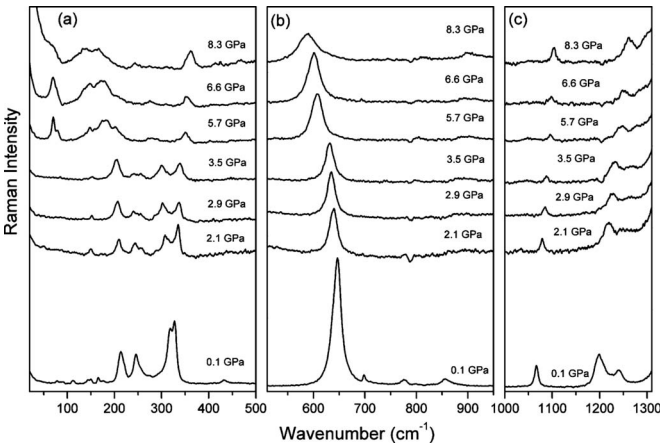

FIG. 6. Raman spectra of KNBO recorded at different pressures during decompression experiments in the (a) low, (b) medium, and (c) high wave-number region.

ture. For instance, in the hexagonal phase the Nb-O2 and Nb-O3 distances (within the *ab* plane, see Fig. 1) are 1.9422 and 2.0087 Å whereas the Nb-O1 distances along the *c* axis are 1.9954 Å.[6] The corresponding distances in the room temperature phase are 1.933–1.946 Å, 2.021–2.026 Å, and 1.803–2.251 Å, respectively.[7] It can be noticed that the Nb-O distances within the *ab* plane are very similar for both phases. However, in the room-temperature phase one of the Nb-O distances along the *c* axis becomes shorter while the other much longer when compared to the hexagonal phase. These changes can be mainly related to significant shifts of the Nb atoms away from the center of the NbO_6 octahedra mainly along the *c* axis. Dielectric and Brillouin studies also suggested that ferroelectric properties of this material are determined by several interacting mechanisms of polar ordering.[8,10] One of the mechanism is a change in the degree of ordering in the potassium sublattice but another mechanism may be related to the dipole formation in the NbO_6 sublattice.[8,10]

As mentioned above the most characteristic changes at 1.2 GPa are: (i) disappearance of the 113.6, 165.6, 179.2, and 271.6 cm^{-1} bands, (ii) very clear changes in the slope of wave numbers vs pressure for majority of modes, (iii) weak discontinuities in the pressure dependence of wave numbers for majority of modes, and (iv) significant decrease in intensity of the 697.7 cm^{-1} band. The comparison of the pressure-dependent Raman spectra with our previous temperature-dependent Raman spectra shows that the observed changes at 1.2 GPa are similar to the changes observed at ambient pressure and 185 K.[11] Present results indicate that the phase-transition temperature increases with increasing pressure and the phase stable above 1.2 GPa is the same as that observed below 185 K. The symmetry of this phase is unknown, therefore it is not possible to discuss the mechanism of this phase transition. The obtained results show that a few low wave-number modes, which can be attributed mainly to translational motions of the K atoms, disappear at 1.2 GPa suggesting the driving force of the phase transition at 1.2 GPa is most likely displacements of the K atoms toward the center of the potassium-oxygen polyhedra. These potassium atoms are located in large pentagonal prismatic cavities (see Fig. 1) and at room temperature the K atoms are significantly shifted from the center of the potassium-oxygen polyhedra within the *ab* plane.[6,7] Our results show that the application of pressure leads to significant compression of the crystal structure within the *ab* plane (in hexagonal notation), as evidenced by large and positive α coefficients for the stretching modes of the planar BO_3 groups lying within the *ab* plane (see Table IV). As a result, the size of the large pentagonal cavities occupied by the potassium atoms diminishes, which leads to significant shifts of the potassium ions within the *ab* plane.

Although displacements of the potassium atoms seems to be the driving force of the observed phase transition, our results also show significant changes in the 200–330 cm^{-1} modes, which involve strong contribution of bending vibrations of the NbO_6 octahedra and translational motions of the Nb atoms. Furthermore, changes are also observed for the 645.6 cm^{-1} band attributed to a stretching mode of the NbO_6 octahedra, which suggests that the Nb atom displacements also play an important role in the pressure-induced phase transition. It is worth noting that the majority of modes, which correspond to vibrations of the NbO_6 octahedra, exhibit negative pressure dependence. This effect can be very clearly observed, for instance, for the stretching mode at 645.6 cm^{-1}. The origin of this negative pressure dependence may be related to the high-pressure Raman results published for simple ABO_3 perovskites. Phase transitions in simple perovskites can be approximated by (i) a rotation (tilt) of the BO_6 octahedra and (ii) A and/or B cation displacements.[24,27] High-pressure Raman studies of $NaNbO_3$, $SrTiO_3$, and $LaAlO_3$, which exhibit phase transitions associated with tilts of the BO_6 octahedra, show positive pressure dependence of the most intense Raman band near 600–650 cm^{-1} and nearly all other modes.[24,28,29] However, a negative pressure dependence for the most intense Raman band at 600–650 cm^{-1} and many bands in the low wave-number region was observed for $KNbO_3$, $BaTiO_3$, and $PbTiO_3$.[22,30,31] This negative pressure shift was attributed to diminishing of the B cation displacement from the center of the BO_6 octahedra.[22,30,31] In case of $KNbO_3$, the transition into paraelectric cubic phase with totally symmetric NbO_6 octahedra occurs at 9–10 GPa with cubic phase modes exhibiting the usual hardening with increasing pressure.[22] Therefore it is plausible to assume that the observed negative pressure dependence for majority of KNBO modes, which were attributed to NbO_6 groups, is related to decrease in the NbO_6 distortion with increasing pressure. As mentioned above, in the room-temperature phase the Nb atoms are significantly shifted from the center of the NbO_6 octahedra along the *c* axis forming one very short (near 1.8 Å) and one very long (near 2.2 Å) Nb-O distance along this axis [these distances correspond to the Nb-O1 distance in the hexagonal phase (1.9954 Å)]. Therefore a decrease in the octahedral distortion along the *c* axis means that the Nb atoms shift toward the center of the NbO_6 octahedra and as a result the short Nb-O distance becomes significantly longer. It is worth noting that an increase in the short Nb-O distance directed along the *c* axis explains the observed softening of the 645.6 cm^{-1} mode since our calculations show that this mode involves

TABLE IV. Raman wave numbers ω_0 for the three phases of $K_3Nb_3B_2O_{12}$ along with pressure coefficients α obtained from the linear fits on the data to $\omega(P)=\omega_0+\alpha P$.

Ambient pressure phase		Intermediate phase		High-pressure phase	
ω_0 (cm^{-1})	α (cm^{-1} GPa^{-1})	ω_0 (cm^{-1})	α (cm^{-1} GPa^{-1})	ω_0 (cm^{-1})	α (cm^{-1} GPa^{-1})
1240.2	12.6	1244.1	7.9	1258.2	5.0
1201.4	8.8	1201.4	8.7	1218.9	5.0
1066.9	7.5	1068.6	5.3	1080.5	2.7
856.3	7.6	855.2	6.1		
		817.9	2.6		
		794.3	1.5	781.7	3.7
775.7	4.0	779.3	0.1		
697.7	−0.8	697.1	−0.6		
645.6	−5.4	646.8	−4.0	656.0	−8.2
433.1	1.0	430.1	4.0	414.9	6.3
410.1	2.1	410.2	−0.3	387.3	3.5
328.1	2.1	327.7	3.1	321.3	5.1
		318.5	2.7	320.2	4.6
317.2	−3.5	315.1	−3.9	297.8	1.6
296.9	4.8	294.6	−1.5		
271.6	1.2			258.1	2.3
256.7	0.9	257.0	−0.4		
245.4	−2.2	247.2	−1.7	211.7	3.8
220.0	0.1	214.4	2.6		
214.2	−1.1	219.2	−2.8	190.6	1.4
				214.9	−3.5
179.2	−0.1			200.6	−3.5
165.6	2.6				
146.1	3.1	147.1	1.7	157.9	−0.1
138.5	3.6	128.6	2.0	177.2	−4.8
				195.7	−9.1
113.6	1.1				
78.6	−0.4	92.8	−2.2	90.8	−2.1
				85.2	−2.2

large vibrations of mainly the O1 atoms in the direction parallel to the *c* axis.

Figure 4 shows that the pressure dependence of stretching modes of the BO_3 groups is significantly weaker between 1.2 and 4.5 GPa compared to 0–1.2 GPa range. This result indicates that the intermediate phase is less compressible within the *ab* plane than the ambient pressure phase. However, the majority of modes corresponding to vibrations of the NbO_6 octahedra exhibit strong and negative pressure dependence. This result indicates that increasing pressure above 1.2 GPa leads to further decrease in the NbO_6 distortion. At 4.5 GPa, a phase transition takes place, as evidenced by clear jumps in $\omega(P)$ observed for many modes (see Fig. 4). Presence of clear jumps suggests that this transition has most likely a first-order character. Since the largest jumps are observed for the modes assigned to the NbO_6 groups whereas the stretching modes of the BO_3 groups show only small kinks, we suppose that this transition is associated mainly with shift of the Nb atoms. However, the FWHM of the symmetric BO_3 stretching mode strongly increases near 4.2 GPa (see Fig. 5) indicating that this mode is also involved in the phase transition, i.e., the BO_3 groups are also affected by this transition. Our results also show that the number of observed modes is similar for the intermediate and high-pressure phases. There is also no indication of any coalescence of modes. These facts suggest that the symmetry of the high-pressure phase is still lower than hexagonal.

When pressure increases above 4.5 GPa, a very broad multicomponent band appears between 100 and 200 cm^{-1}. Moreover, a central peaklike feature (quasielastic scattering) appears above 4.5 GPa. Interestingly, similar very broad band was observed in the high-pressure Raman scattering studies of $KNbO_3$ close to the transition into the paraelectric cubic phase.[21,22,32] Since the Raman spectra above 4.5 GPa show clear bands associated with the lattice modes, a long-range order is preserved and the strong broadening of bands

cannot be attributed to partial amorphization of the sample. Presence of the quasielastic scattering and strong broadening of Raman bands corresponding to the NbO_6 units indicate that in the high-pressure phase the Nb atoms are dynamically disordered among symmetry equivalent positions displaced from the average lattice site, i.e., the correlation between off-center shifts of Nb atoms is suppressed. Interestingly, many modes of the high-pressure phase still exhibit negative pressure dependence (see Table IV). For the 645.6 cm^{-1} mode, the pressure dependence is even more pronounced than that observed below 4.5 GPa. The softening of these modes indicates that the Nb atoms shift further toward center of the NbO_6 octahedra with increasing pressure revealing that this high-pressure phase is still not stable, i.e., it is very likely that it will transform to yet another phase above 8.3 GPa, the highest pressure reached in our experiment.

IV. CONCLUSIONS

Lattice-dynamics calculations and high-pressure Raman studies were performed on KNBO. Assignment of the observed Raman peaks to definite atomic motions was proposed. Pressure-dependent studies revealed successive pressure-induced phase transitions at around 1.2 and 4.5 GPa. The first transition is most likely associated with significant shift of the potassium atoms toward the center of the potassium-oxygen polyhedra accompanied by weak decrease in the NbO_6 distortion. The second transition in KNBO is related mainly to significant changes at the niobium-oxygen sublattice, i.e., shifts of the Nb atoms toward center of the NbO_6 octahedra. Since displacement of the Nb atoms is responsible for ferroelectric properties of the perovskite-type materials, our results show that pressure suppresses ferroelectric order in KNBO crystals. In the high-pressure phase stable above 4.5 GPa the niobium atoms are disordered, as evidenced by large bandwidth of Raman bands and appearance of quasielastic scattering. Our results also show that compressibility within the *ab* plane decreases when going from the ambient pressure to high-pressure phase. This result points to significant decrease in size of the pentagonal cavities occupied by the potassium ions.

Interestingly, the observed behavior of KNBO as a function of pressure is to some extent similar to the behavior of simple perovskites, in spite of large structural differences between these materials. In particular, similarly as for simple ABO_3 perovskites with larger compressibility of the AO_{12} polyhedra than BO_6 octahedra, the Nb (B) atom displacement decreases with increasing pressure. However, KNBO is softer and the observed softening of the NbO_6 stretching mode near 600–650 cm^{-1} is more pronounced due to less compact arrangements of the structural units in the KNBO structure.

ACKNOWLEDGMENTS

Brazilian authors acknowledge Brazilian Agencies CAPES, FUNCAP, and CNPq for partially supporting this research.

[1] A. A. Kaminskii, P. Becker, L. Bohaty, S. N. Bagaev, H. J. Eichler, K. Ueda, J. Hanuza, H. Rhee, H. Yoneda, K. Takaichi, I. Terashima, and M. Maczka, Laser Phys. **13**, 1385 (2003).
[2] G. Aka, A. Kahn-Harari, F. Mougel, D. Vivien, F. Salin, P. Coquelin, P. Colin, D. Pelenc, and J. P. Damelet, J. Opt. Soc. Am. B **14**, 2238 (1997).
[3] J. F. H. Nicholls, B. Henderson, and B. H. T. Chai, Opt. Mater. **16**, 453 (2001).
[4] X. B. Hu, J. Y. Wang, C. Q. Zhang, X. G. Xu, C. K. Loong, and M. Grimsditch, Appl. Phys. Lett. **85**, 2241 (2004).
[5] A. A. Kaminskii, P. Becker, L. Bohaty, H. J. Eichler, A. N. Penin, K. Ueda, J. Hanuza, K. Takaichi, and H. Rhee, Phys. Status Solidi A **201**, 2154 (2004).
[6] P. Becker, L. Bohaty, and J. Schneider, Kristallografiya **42**, 250 (1997).
[7] P. Becker, P. Held, and L. Bohaty, Z. Kristallogr. **211**, 449 (1996).
[8] V. I. Voronkova, E. P. Kharitonova, V. K. Yanovskii, S. Yu. Stefanovich, A. V. Mosunov, and N. I. Sorokina, Crystallogr. Rep. **45**, 816 (2000).
[9] E. P. Kharitonova, V. I. Voronkova, V. K. Yanovskii, and S. Yu. Stefanovich, Neorg. Mater. **38**, 819 (2002).
[10] M. Mączka, J. Hanuza, and S. Kojima, Phys. Rev. B **77**, 104116 (2008).
[11] M. Mączka, K. Hermanowicz, and J. Hanuza, J. Phys.: Condens. Matter **17**, 3355 (2005).
[12] H. K. Mao, P. M. Bell, J. W. Shaner, and D. J. Steinberg, J. Appl. Phys. **49**, 3276 (1978).
[13] J. D. Gale, J. Chem. Soc., Faraday Trans. **93**, 629 (1997).
[14] M. Mączka, W. Paraguassu, A. G. Souza Filho, P. T. C. Freire, F. E. A. Melo, J. Mendes Filho, and J. Hanuza, J. Raman Spectrosc. **36**, 56 (2005).
[15] G. D. Saraiva, W. Paraguassu, M. Maczka, P. T. C. Freire, J. A. Lima, C. W. A. Paschoal, J. Mendes Filho, and A. G. Souza Filho, J. Raman Spectrosc. **39**, 937 (2008).
[16] M. Maczka, J. Hanuza, W. Paraguassu, A. G. Souza Filho, P. T. C. Freire, and J. Mendes Filho, Appl. Phys. Lett. **92**, 112911 (2008).
[17] E. Dowty, Phys. Chem. Miner. **14**, 67 (1987).
[18] H. R. Xia, L. X. Li, J. Y. Wang, W. T. Yu, and P. Yang, J. Raman Spectrosc. **30**, 557 (1999).
[19] A. de Andrés, F. Agullo-Rueda, S. Taboada, C. Cascales, J. Campa, G. Ruiz-Valero, and I. Rasines, J. Alloys Compd. **250**, 396 (1997).
[20] M. Mączka, J. Hanuza, A. Pajaczkowska, Y. Morioka, and J. H. Van der Maas, J. Raman Spectrosc. **35**, 266 (2004).
[21] Z. X. Shen, Z. P. Hu, T. C. Chong, C. Y. Beh, S. H. Tang, and M. H. Kuok, Phys. Rev. B **52**, 3976 (1995).
[22] D. Gourdain, E. Moya, J. C. Chervin, B. Canny, and Ph. Pruzan, Phys. Rev. B **52**, 3108 (1995).
[23] Y. Shiratori, A. Magrez, K. Kasezawa, M. Kato, S. Röhrig, F. Peter, C. Pithan, and R. Waser, J. Electroceram. **19**, 273 (2007).

[24] M. Guennou, P. Bouvier, J. Kreisel, and D. Machon, Phys. Rev. B **81**, 054115 (2010).
[25] M. Maczka, W. Paraguassu, A. G. Souza Filho, P. T. C. Freire, J. Mendes Filho, and J. Hanuza, Phys. Rev. B **77**, 094137 (2008).
[26] M. Maczka, W. Paraguassu, A. G. Souza Filho, P. T. C. Freire, A. Majchrowski, J. Mendes Filho, and J. Hanuza, Phys. Rev. B **78**, 064116 (2008).
[27] R. J. Angel, J. Zhao, and N. L. Ross, Phys. Rev. Lett. **95**, 025503 (2005).
[28] Z. X. Shen, X. B. Wang, S. H. Tang, M. H. Kuok, and R. Malekfar, J. Raman Spectrosc. **31**, 439 (2000).
[29] P. Bouvier and J. Kreisel, J. Phys.: Condens. Matter **14**, 3981 (2002).
[30] U. D. Venkateswaran, V. M. Naik, and R. Naik, Phys. Rev. B **58**, 14256 (1998).
[31] J. A. Sanjurjo, E. Lopez-Cruz, and G. Burns, Phys. Rev. B **28**, 7260 (1983).
[32] M. Md. Shamim and T. Ishidate, Solid State Commun. **113**, 713 (2000).
[33] See supplementary material at http://link.aps.org/supplemental/10.1103/PhysRevB.82.014106 for Lorentzian fitting.